PERGAMON

International Journal of Heat and Mass Transfer 45 (2002) 937–949

International Journal of HEAT and MASS TRANSFER

www.elsevier.com/locate/ijhmt

Laminar–turbulent transition behavior of fully developed air flow in a heated horizontal tube

H. Koizumi *

Department of Mechanical Engineering and Intelligent Systems, The University of Electro-Communications, Chofu, Tokyo 182-8585, Japan

Received 17 February 2001; received in revised form 5 July 2001

Abstract

I have experimentally studied the influence of the buoyancy force and inlet flow conditions on the laminar–turbulent transition process of fully developed air flow in a heated horizontal tube with uniform wall heat flux at modified Rayleigh number 3.1×10^6. Eight time-series of the air temperature were simultaneously obtained using eight thermocouples positioned within the tube along a vertical line passing through the tube's axis. I have studied the time and space dependence of the transition behavior by analyzing these instantaneous time-series. By calculating a set of Lyapunov exponents and the correlation dimension of the time-series of a single thermocouple, these transitional flows are found to be chaotic.

1. Introduction

The laminar–turbulent transition of fluid flow in tubes is encountered in a wide variety of engineering situations, including duct flow and heat exchangers in chemical processes. It is important to elucidate the mechanisms and characteristics of such transitions, because the macroscopic heat and mass transfer performance of fluid flow systems of this type is significantly influenced by these mechanisms and characteristics in the transitional regime. From previous investigations, it is known that there are typically two types of transition processes in this context. One is the so-called "cascade-type transition" in an enclosure, such as in the case of Taylor–Couette flow [1] and Rayleigh–Bénard flow [2], and the other is the so-called "breakout-type transition", such as that in unheated tube flow [3,4]. The transition process of the cascade type has come to be understood through many experimental and numerical studies. This transition process always produces a limit cycle through the first Hopf bifurcation, and then, as the control parameter is increased further, this limit cycle becomes a torus or comes to exhibit period-doubling motion. Further increasing the control parameter results in a series of successive bifurcations and eventually to chaos. In contrast to the situation for the transition process of the cascade type, there is almost nothing known, even experimentally, about the transition process of the breakout type.

With the above-described situation regarding the study of the laminar–turbulent transition, some experimental investigations have been made on this transition in unheated tube flow, which is a typical type of breakout transition. For example, Wygnanski and coworkers [3,4] experimentally found that "puff flow" is produced when the entrance flow is strongly disturbed and the tube is sufficiently long, and "slug flow" is produced when the entrance flow is undisturbed. They determined the regions in which puff flow and slug flow occur in transitional flow as a whole in terms of the disturbance level at the tube entrance, and described the important characteristics of puffs and slugs in full detail. A flow visualization experiment of equilibrium puff flow was reported by Bandyopadhyay [5]. He observed various organized types of motion: high-speed laminar plug flow around the tube axis flowing into the turbulent region near the upstream interface, shedding of a train of wake-like vortices and helical motion near the upstream interface, and longitudinal vortices in the downstream region. Recently, Matsuuchi and Adachi [6]

* Tel.: +81-424-43-5395.
E-mail address: koizumi@mce.uec.ac.jp (H. Koizumi).

0017-9310/02/$ - see front matter
PII: S0017-9310(01)00210-1

Nomenclature

D	tube inner diameter
D_c	correlation dimension
d_m	embedding dimension
Gr_q	modified Grashof number, $g\beta q_w D^4/(\kappa\nu^2)$
Pr	Prandtl number, ν/α
q_w	heat flux at the tube wall
r	distance from the tube axis measured along a line perpendicular to the axis ($r = 0$ corresponds to the tube's axis, and the downward direction is positive: Fig. 1)
R	tube inner radius, $D/2$
Ra_q	modified Rayleigh number, $Gr_q \cdot Pr$
Re	Reynolds number, $U_m D/\nu$
Re_{trans}	transition Reynolds number at which fluctuations first appear
t	time
T	temperature
T_{FI}	fluctuation intensity of fluid temperature, $(\sqrt{T_f'^2/\bar{T}_{fc}}) \times 100$
U	velocity along the axial direction
$U_{FI\ in}$	fluctuation intensity of velocity at the tube inlet, $((\sqrt{U_f'^2/\bar{U}_{fc}}) \times 100)_{in}$
x	axial coordinate (Fig. 1)
	Physical properties were estimated at the bulk fluid temperature of the measuring section

Greek symbols

α	thermal diffusivity of the fluid
β	coefficient of thermal expansion
$\Delta\tau$	time interval of sampling
Θ	nondimensional fluid temperature, $(T_{tw} - T_f)/(T_{tw} - \bar{T}_{fc})$
λ_i	Lyapunov exponents ($i = 1, \ldots, d_m$)
ν	kinetic viscosity of the fluid
τ	axial wall temperature gradient
τ_{del}	delay time
τ_{dev}	evolution time

Subscripts

b	value at the bulk fluid temperature
c	value at the tube axis
f	fluid
m	mean value throughout the tube
tw	value at the top of the tube wall

Overline

$\bar{\bullet}$	time-averaged value of $\bullet$

conducted an experimental investigation to clarify the mechanism of the generation and growth of puff flow in the entrance region. They found that this mechanism is necessary to exist both the turbulent lumps transported with averaged-mean velocity, which have extended spatial structure, and the large-velocity laminar flow along the tube axis. Furthermore, they discovered that the large fluctuation intensities near the entrance gradually become concentrated as the distance from the entrance increases and become quite localized within the tube cross-section beginning at a distance of about 60 times the tube diameter. These turbulent lumps grow into two kinds of puffs, an equilibrium puff, which has structure extending from the tube axis to the tube wall, and a quasi-equilibrium puff, which gradually disappears in the downstream region.

Compared to the extensive research conducted on systems with unheated flow, there have been very few studies focusing on heated flow, and as a result there is an incomplete understanding of many details of the transition process here. Elucidating the characteristics and mechanisms of such transitions is important not only for practical engineering reasons, but also to answer basic scientific questions regarding heat transfer. In a heated horizontal tube, a secondary flow is produced by the buoyancy force in the tube cross-section, and resultingly the transition involves different processes than that in unheated flow. Nagendra [7] studied the time-averaged and statistical nature of heat transfer in the laminar–turbulent transition in a system of combined forced and free convection exhibited by water flowing in a horizontal tube. El-Hawary [8] determined a stability map describing regions of different flows in a plane of nondimensional coordinates representing forced and free convection effects in horizontal water flow. More recently, Abid et al. [9,10] performed measurements providing a detailed description of the wall temperature change along both the azimuthal and axial directions using infrared thermography in horizontal water flow with uniform wall heat flux. They elucidated the nature of the laminar–turbulent transition process in terms of its spatio-temporal behavior from the entrance to the fully developed regime. They also determined the time evolution of the fractal dimension for various Reynolds numbers and as a function of the distance along the axial coordinate. In a typical case, they found that the fractal dimension begins near the tube inlet with a value greater than 12 and decreases along the axial coordinate to about 3 in the fully developed regime for $Re = 2600$. However, they did not measure the flow field directly, and thus their results leave many unanswered questions. Furthermore, there is the possibility that the values they obtained as a time-series of the tube wall temperature may have been significantly reduced owing to the tube's large heat capacity. (Their tube was of 0.2 mm thickness and 9.6 mm inner diameter.) Therefore, it

is likely that the results of Abid et al. [9,10] do not accurately describe the real transition behavior. In particular, the fractal dimensions of the attractor they obtained by analyzing the time-series of the tube wall temperature are suspicious. Obtaining the proper description of the real transition characteristics provided the motivation of the present work and the direct measurement of the flow fields. I hope this will produce a clear picture of the characteristics and mechanisms of the laminar–turbulent transition of a heated horizontal tube flow.

The aim of this experimental study is to reveal the influence of the buoyancy force and inlet flow conditions on the laminar–turbulent transition behavior in fully developed air flow in a heated horizontal tube with uniform wall heat flux. Also, I attempt to gain an understanding of the transition process in terms of the chaotic behavior of a nonlinear dynamical system by analyzing the observed time-series of the sensor output.

2. Experimental apparatus and techniques

2.1. Experimental apparatus

Fig. 1 presents a schematic drawing of the experimental apparatus and the coordinate system. The working medium was air (Prandtl number $Pr = 0.71$), which was compressed by a blower and sent into a long, straight horizontal tube downstream of a settling chamber. I positioned a flexible tube between the blower and the straight tube to prevent transmission of the blower's vibration. The straight tube was in total 13 m ($228D$, where D is the inner diameter of the tube) long, and all tubes were made of brass of 1.5 mm thickness and 57 mm inner diameter. The heated test section was 10 m long ($175D$). In front of this was situated an unheated length of 3 m ($53D$) serving as a hydrodynamic approach. The heated section was electrically heated with a uniform wall heat flux $q_w = 340$ W/m^2, and the modified Rayleigh number was $Ra_q = 3.1 \times 10^6$. The flow rate of air was measured by a float-area-type flow meter. The flow Reynolds number was adjusted by varying the flow rate, and I could set the value of Re with a precision of about ± 5 by placing three flow meters of measuring ranges 0.2–2.0, 3–30 NL/min and 2–20 Nm^3/h along a line. In order to investigate the effect of the inlet flow conditions on the transition process, two different velocity fluctuation intensities were used, $U_{FI\ in} = 1.2\%$ and $U_{FI\ in} \approx 40\%$. These were realized, respectively, with and without a turbulence generator placed at the tube inlet.

Thermocouples of 0.1 mm in diameter were soldered to the outer surface of the tube at some fixed intervals in both the axial and azimuthal directions. These measured the axial wall temperature gradients of the heated tube

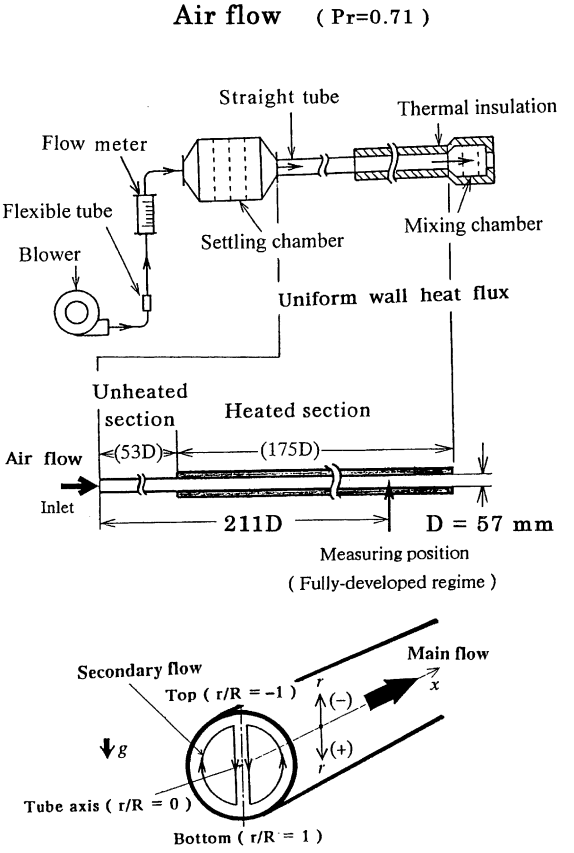

Fig. 1. A schematic drawing of the experimental apparatus and coordinate system.

wall. The bulk temperature of the fluid in the outlet section was measured by attaching a mixing chamber to the heated tube with a flange. Fig. 2 displays the axial

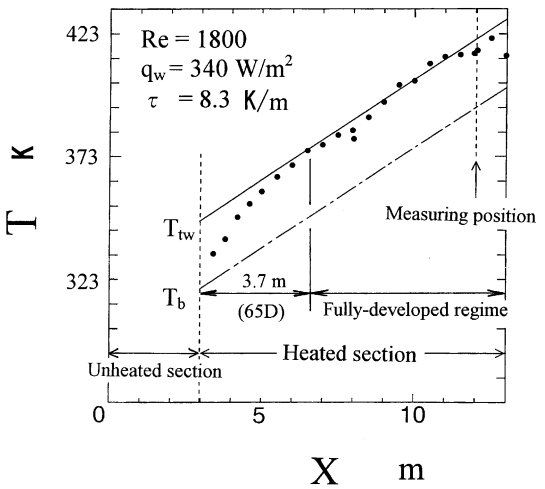

Fig. 2. Axial wall temperature gradient of the heated tube.

temperature gradients of the heated tube. The solid dots in the figure represent the measured temperatures at the top of the tube outer wall. The fitted solid line corresponds to a constant axial wall temperature gradient of $\tau = 8.3$ K/m beginning at a position about 3.7 m ($65D$) downstream from the beginning of the heated section. This gradient is almost identical to the measured temperature gradient of the bulk fluid temperature, indicated by the dot-and-dashed line. Therefore, I confirmed that a uniform wall heat flux was obtained and that the position at which the macroscopic flow and temperature fields were measured was in the fully developed flow regime.

2.2. Measurement of temperature and velocity fields

The fluid temperature was measured by a thermocouple (abbreviated as 'TC'). The diameter of its copper and constantan wires was 25 μm, and the response time was about 0.05 s. The fluid velocity was measured by a hot-wire anemometer (abbreviated as 'HWA'). The diameter of its tungsten wire was 7 μm. These probes were inserted into the tube through a hole in its upper wall, and they were positioned to intersect the midplane. The TC was such that its sensing point lay 6 mm upstream of a supporting thin stainless L pipe of 1 mm outer diameter. The measuring position of the temperature and velocity fields was in the fully developed flow section, $211D$ downstream from the tube inlet. I sampled 30,000 data points from the time-series generated by the TC and HWA using a 12-bit analog-to-digital converter. The time-averaged values and fluctuation intensities of the temperature and velocity were obtained by processing these data using a microcomputer. Also, the power spectrum of the temperature fluctuations was obtained by analyzing the output of the TC using an FFT analyzer. I found that the TC had a sufficiently short response time to follow the turbulence signatures, from the power spectra at $Re = 2230$ shown in Fig. 10(b), by confirming that almost identical power spectra were obtained using a HWA. (I did not separate the output of the HWA into velocity and temperature components.)

In order to clarify the relation between the nature of the turbulent signature and the instantaneous velocity and temperature profiles, I attempted to obtain the instantaneous temperature profile by positioning eight TCs inside the tube along a vertical line intersecting the tube axis. In this way, eight time-series of the air temperature were simultaneously obtained using a microcomputer. This multi-TC probe was inserted into the tube from the oval-shaped hole in its upper wall. This hole was then blocked using a cover sheet and insulating material wrapped around the tube. The horizontal position of this set of TCs was such that their sensing points lay 6 mm upstream of a set of eight supporting thin stainless L pipes of 1 mm outer diameter. The radial positions of the points at which the temperature was measured were $r/R = \pm 0.12, \pm 0.37, \pm 0.61, \pm 0.86$, symmetrically positioned about the tube axis. I elucidated the nature of the transition behavior in space and time by analyzing these instantaneous time-series.

2.3. Lyapunov exponents and phase space

I obtained the Lyapunov exponents λ_i from the observed time-series of the TC. These exponents λ_i $(i = 1 - d_m)$ represent the rate at which the magnitude of the displacement vector between two neighboring points in phase space grows in time. The exponents can be calculated by the method proposed by Zeng et al. [11]. This algorithm uses a shell rather than a ball to minimize the effects of noise or measurement error inherent in many experimental situations. When the volume of phase space is normalized to unity, the inner radius of such a shell is given by $\varepsilon_{r\ \min} = 0.02$ (This represents the length scale of the noise.) and the outer radius is given by $\varepsilon_{r\ \max} = 0.05$. When one or more positive exponents are obtained, the flow is considered to be chaotic, with the magnitude of the exponents indicating the time-scale of predictability.

From the time-series of a TC, an attractor was reconstructed in a d_m-dimensional phase space. Then I obtained the λ_i from the orbits of points evolving in time interval of length τ_{dev}. I sampled 131,072 data points from a time-series of TC using a 16-bit analog-to-digital converter, and the sampling time $\Delta\tau$ was set to 0.01953 s. All calculations were carried out on a workstation. A detailed description of the analyzing method is given in a previously published paper [12].

2.4. Correlation dimension

The correlation dimension, D_c, represents the complexity of strange attractors. D_c can be calculated with the method proposed by Grassberger et al. [13] using a time-series of the fluid temperature $\{T_i = T(i\Delta\tau)\}$ with $i = 1, 2, \ldots, M$, where M is the number of observations and $\Delta\tau$ is the time interval of sampling. An attractor can be reconstructed in d_m-dimensional phase space by an embedding. To determine D_c, first a locus point T_i from an arbitrary point of phase space was chosen as the center of a small ball ε_r. The number of locus points T_j contained in this ball is N. The definition of the correlation integral corresponding to this ball is

$$C(\varepsilon_r) = \frac{1}{N^2} \sum_{i,j=1}^{N} H(\varepsilon_r - \|T_i - T_j\|),$$

where $H(x)$ is the Heaviside function. For sufficiently small ε_r, the function $C(\varepsilon_r)$ can be fit to a power of ε_r (that is, in the limit that $N \to \infty$, $C(\varepsilon_r)$ approaches an analytic function), and D_c is defined as this power:

$C(\varepsilon_r) \propto r^{D_c}$. Therefore, D_c can be obtained as $D_c = \lim_{\varepsilon_r \to 0}(\ln C(\varepsilon_r)/\ln(\varepsilon_r))$.

2.5. Flow visualization

I allowed for the visualization of an instantaneous velocity profile in the transitional regime along the axial direction using a smoke-wire method. I attached a transparent acrylic tube of 500 mm length to the end of the heated brass tube with a flange to facilitate flow visualization. The diameter of the nichrome wire used for this purpose was 0.1 mm, and the wire was positioned within the tube along a vertical line passing through the tube's axis 10 mm downstream from the entrance of the acrylic tube. A photograph was taken 33 ms after the smoke was produced. A strobe scope was used for lighting, and at the same time the shutter was automatically released with a speed of 1/15 s.

3. Results and discussion

3.1. Velocity and temperature fields in the steady laminar regime

Before analyzing the transition regime, I determined the steady laminar velocity and temperature fields in the case of unheated flow to check the accuracy with which the experimental apparatus was assembled and, in the case of heated flow, to examine the discrepancy between the temperature distribution observed experimentally [14] and that found in numerical simulation [16].

3.1.1. Unheated flow

I obtained the velocity distributions using a HWA along vertical and horizontal directions within the tube in the fully developed measuring section for unheated flow at $Re = 1800$, and I confirmed that these distributions are in quantitative agreement with those of Poiseuille flow within a precision of about 3%.

3.1.2. Heated flow

I obtained the velocity distribution using a Pitot tube and the temperature distribution using a TC by measuring these quantities at a number of points along a vertical line passing through the tube's axis. During heating, fluid near the wall is warmer and therefore lighter than the bulk fluid in the center part of the tube. The resulting upward flows moving along the inside of the tube converge at the top of the tube, where they join and form a downward flow in the central part of the tube. In this way, a pair of vortices is created. This pair is symmetric with respect to reflection about the vertical plane passing through the tube's axis. Due to this secondary flow, a point of maximum velocity exists in the lower region around $r/R = 0.7$. It is known that velocity and temperature distributions in the steady laminar regime are functions of the product of the Reynolds and Rayleigh numbers for a fixed Prandtl number, as found in the boundary-layer analysis of Mori et al. [14,15] for large Rayleigh number.

Fig. 3 displays the measured nondimensional velocity distribution U/U_c and temperature distribution Θ_f along a vertical line passing through the center of the tube for $ReRa_\tau = 0.89 \times 10^5$. (Here $Re = 980$, and the axial wall temperature gradient of the tube is $\tau = 3$ K/m. In the laminar flow regime I use the Rayleigh number of $Ra_\tau = g\beta\tau R^4/\alpha\nu$, where R is the inside radius of the tube, to facilitate comparison with the results of other papers [14,16].) Here, Fig. 3(a) represents the results for U/U_c, and Fig. 3(b) those for Θ_f. The circles represent my experimental results, while the triangles represent those of Mori et al. [14], and the dotted curves are the numerical results of Ishigaki and Mochizuki [16] for air flow.

As I see in the figure, there exists a discrepancy in the distributions of Θ_f, especially in the upper part of the tube, between the experimental result of Mori et al. [14] as indicated by the triangles, and the numerical results of Ishigaki and Mochizuki [16] as indicated by the dotted line. The present results, indicated by the circles, are close to the numerical results, and I confirmed that Θ_f in the upper part of the tube increases (T_f decreases) if the amount of insulation is insufficient around the point where the sensor is inserted. I found that the temperature difference between the top and the bottom of the tube wall was about 1–2 K in the measuring section. Since the numerical results were derived from the equations describing only the flow field, in order to take into account the mixed convection phenomenon in full detail, it is necessary to also include a description of the thermal behavior of the tube in numerical simulation, in particular for high Rayleigh numbers.

3.2. Transition characteristics for unheated flow

I determined the transition Reynolds number Re_{trans} at which the appearance of turbulent fluctuations was detected in the output of the HWA.

Fig. 4 displays the time-series of the fluid velocity for unheated flow at the tube's axis ($r/R = 0.00$) for two different inlet flow conditions. Here, Fig. 4(a) displays the turbulent signature that appears around $Re_{trans} = 4600$ for the case of a small inlet fluctuation intensity, $U_{FI\ in} = 1.2\%$, while Fig. 4(b) is the turbulent signature that appears around $Re_{trans} = 2100$ for a large inlet fluctuation intensity, $U_{FI\ in} \approx 40\%$.

Wygnanski and Champagne [3] referred to the turbulent signatures occurring for the case of small $U_{FI\ in}$ as "slugs", and to those for larger values as "puffs". The leading front of the turbulent puff does not have a clearly defined interface, and the trailing front of which

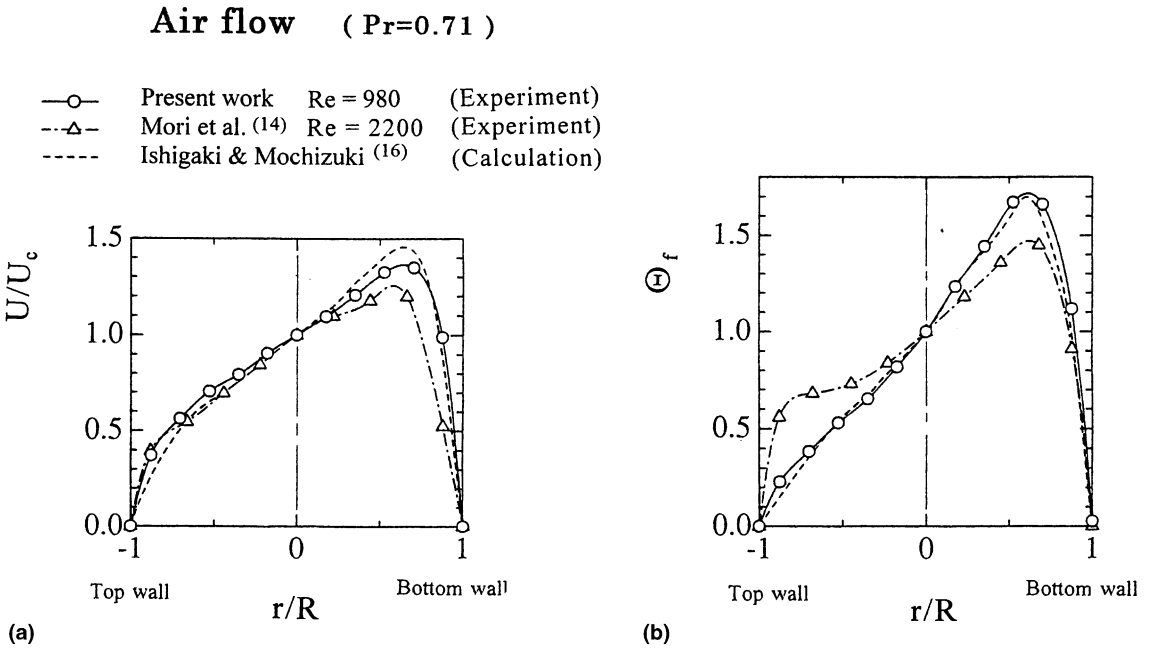

Fig. 3. Nondimensional velocity and temperature distributions at $ReRa_\tau = 0.89 \times 10^5$ in the laminar regime. (a) Velocity distributions. (b) Temperature distributions.

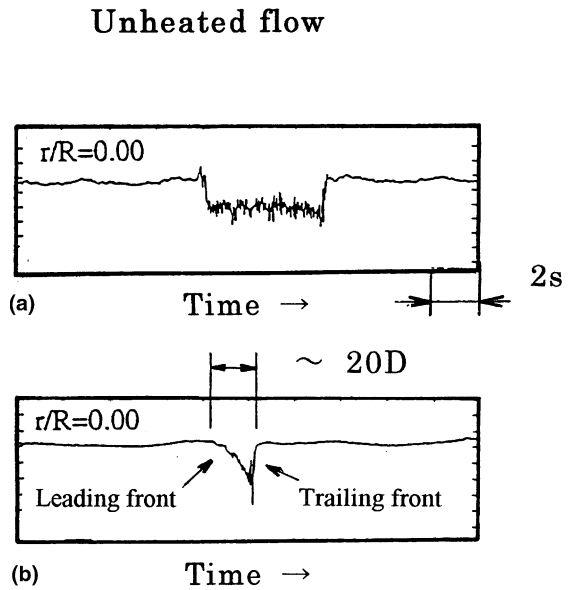

Fig. 4. Hot-wire traces for two inlet flow conditions at $r/R = 0.00$ for unheated flow. (a) Turbulent slug ($Re = 4600$, $U_{FI\ in} = 1.2\%$). (b) Turbulent puff ($Re = 2100$, $U_{FI\ in} \approx 40\%$).

boundary is clearly defined. I confirmed here that the nature of the turbulence signature depends strongly on the level of disturbance at the tube inlet, and my results are in qualitative agreement with those of Wygnanski et al.

3.3. Transition characteristics for heated flow

The experimental investigation for heated transitional flow was carried out at modified Rayleigh number $Ra_q = 3.1 \times 10^6$.

3.3.1. Dependence of the transition behavior on the inlet flow conditions

Below Reynolds number 1900, the flow is completely steady and laminar for the two different inlet flow conditions, $U_{FI\ in} = 1.2\%$ and $U_{FI\ in} \approx 40\%$. Small temperature fluctuations of frequency slightly less than about 1 Hz appear at approximately $Re = 1900$, near the point at which Θ_f is maximal (that is, near $r/R = 0.6$ to 0.7, which also corresponds to the point of maximal velocity). Further increasing the Reynolds number, turbulent lumps that resemble the "turbulent puffs" seen in unheated flow, as shown in Fig. 4(b), appeared intermittently. The appearance of these turbulent lumps is independent of the fluctuation intensity at the tube inlet $U_{FI\ in}$. That is, when Ra_q is large, the secondary flow, caused by buoyancy, leads to the transition at a Reynolds number Re_{trans}, and the value of Re_{trans} depends very little on the fluctuation intensity at the tube inlet.

Fig. 5 displays the hot-wire traces at $Re = 2230$ and $r/R = 0.70$ for the two different inlet flow conditions. (I

did not separate the output of the HWA into velocity and temperature components.) Here, Fig. 5(a) is the result for $U_{FI\ in} = 1.2\%$ and Fig. 5(b) that for $U_{FI\ in} \approx 40\%$. I see that the two time-series are almost identical. The leading front of the turbulent lump here does not have a clearly defined interface, and the trailing front of which boundary is clearly defined. These time-series resemble that of the turbulent puff displayed in Fig. 4(b), which was produced with large $U_{FI\ in}$ for unheated flow. I refer to the large fluctuations in heated flow shown in Fig. 5 as "turbulent lumps resembling turbulent puffs", because their signature resembles that of puffs in unheated flow. However, I could not elucidate the details of these fluctuations and determine the difference between a puff and a lump in this experiment. However, their resemblance suggests that the mechanisms by which they are produced are very similar. That is, the upstream laminar fluid continuously enters the slower-moving turbulent lump, and large fluctuations are thereby produced at the trailing interface of the turbulent lump in the heated flow. In the present experiment, in which turbulent lumps were conveyed with the mean axial velocity U_m, the total axial length of these lumps shown in the Figs. 5(a) and (b) was approximately $30D$. Based on the time-series of the HWA output, no splitting or merging of turbulent lumps, which exist just in the upstream or downstream portions, was observed to take place. This suggests that a turbulent lump is stable and possesses a self-sustaining mechanism, consists of the balance between the production and dissipation of energy, as in the case of a turbulent puff in unheated flow [3,4,6]. This stable structure flows in the downstream direction, maintaining in a near-equilibrium state.

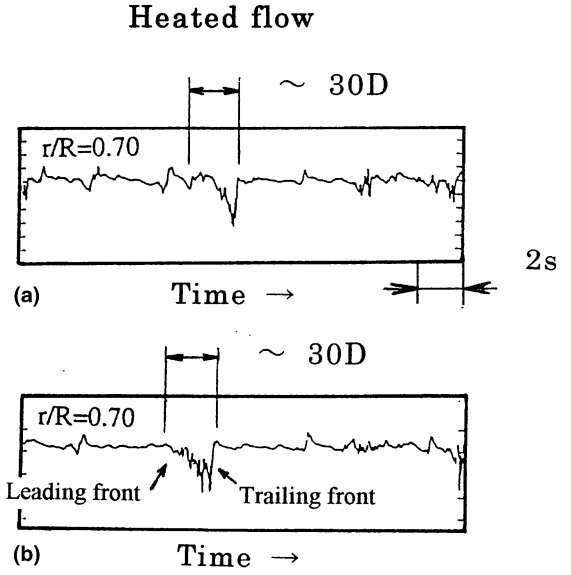

Fig. 5. Hot-wire traces for the two inlet flow conditions at $Re = 2230$ and $r/R = 0.70$ for heated flow. (a) Turbulent lump resembling turbulent puff ($U_{FI\ in} = 1.2\%$). (b) Turbulent lump resembling turbulent puff ($U_{FI\ in} \approx 40\%$).

Mori et al. [14] experimentally found in a similar flow system that, for large $U_{FI\ in}$, the transition Reynolds number Re_{trans} starts at about 2000 and increases with Rayleigh number Ra_τ, while for small $U_{FI\ in}$ Re_{trans} reaches a value as high as about 7700 and decreases with Ra_τ. Furthermore, when the product of Re and Ra_τ is large, the secondary flow created by buoyancy causes Re_{trans} to tend to a single value, independent of $U_{FI\ in}$. My experimental results confirm that the value $Re_{trans} \approx 1900$ and the time-series at $Re = 2230$ are independent of $U_{FI\ in}$ for Rayleigh numbers $Ra_q = 3.1 \times 10^6$, as used in this experiment. Therefore, I carried out the rest of the experiment using only the large $U_{FI\ in}$ value.

Bandyopadhyay [5] pointed out that the most important factor for the generation and growth of puffs in unheated tube flow is the large velocity difference at the laminar-to-turbulent trailing interface of the turbulent lump. Since strong secondary flow is produced from the heated entrance regime, especially in the case of large Rayleigh number flow, the axial velocity exhibits a convex-shaped distribution, with maximum velocity near the bottom wall. Such a velocity profile may result in almost the same time-series of turbulent lumps, which is independent of $U_{FI\ in}$, but further investigation in the heated entrance regime are certainly needed.

3.3.2. Time-averaged characteristics and time-series in the initial transition regime

Fig. 6 displays the time-averaged characteristics and time-series in the initial transition regime. Fig. 6(a) exhibits the nondimensional time-averaged temperature distribution $\bar{\Theta}_f$ and the fluctuation intensity of the fluid temperature T_{FI} at $Re = 1020$, 2170 and 2230. The circles in the figure indicate the results for $Re = 1020$ in the laminar regime, while the solid dots indicate the results for $Re = 2170$ and solid triangles those for $Re = 2230$ in the initial stage of the transition. In Fig. 6(b) are the time-series of the fluid temperature at various radial positions for $Re = 2170$ and 2230.

For values of Re ranging from $Re_{trans} \approx 1900$ to $Re = 2170$, small fluctuations appear only in the lower part of the tube $r/R = 0.1$ to 0.8. The maximum value of the fluctuation intensity of the fluid temperature T_{FI} is about 0.4% at $Re = 2170$ and $r/R = 0.6$ to 0.7, but the fractional form of the time-averaged fluid temperature $\bar{\Theta}_f$, indicated by the solid dots is almost identical to that for laminar flow, indicated by the circles, at $Re = 1020$ shown in Fig. 6(a).

For $Re = 2230$, there appear two maximum values in the fluctuation intensity of the fluid temperature T_{FI}, near $r/R = -0.4$ ($T_{FI} \approx 0.8\%$) and 0.7 ($T_{FI} \approx 1.6\%$). It is

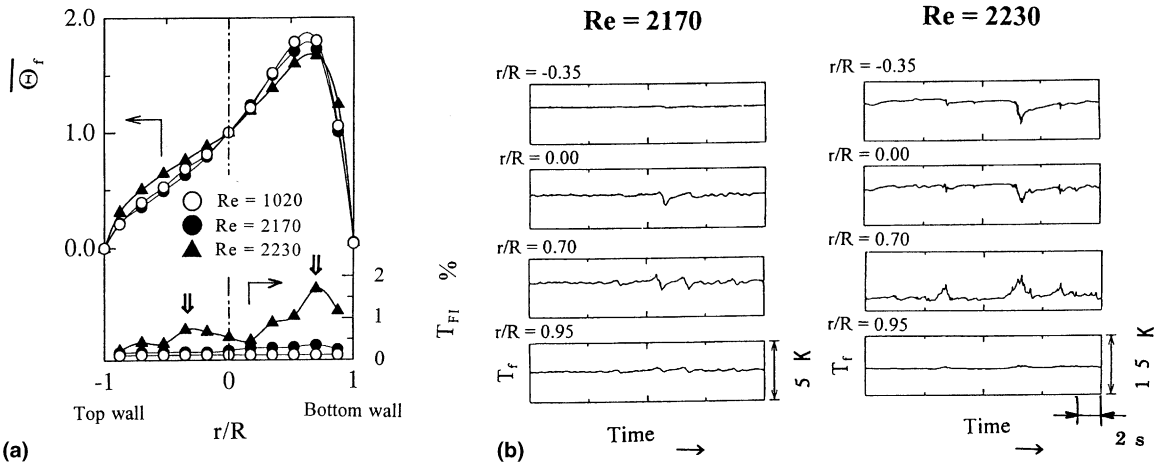

Fig. 6. Nondimensional time-averaged temperature distribution, the fluctuation intensity and time-series of the fluid temperature. (a) Nondimensional time-averaged temperature distribution and the fluctuation intensity of the fluid temperature. (b) Time-series of the fluid temperature at $Re = 2170$ and $Re = 2230$.

found from the time-series shown in Fig. 6(b) that a region of higher temperature with large fluctuations appears intermittently at $r/R = 0.70$, and almost simultaneously a region of lower temperature appears at around $r/R = 0.0$ to -0.35. In order to reveal the temporal and spatial transition behavior, eight time-series of the fluid temperature were compiled using eight thermocouples in the tube positioned along a vertical line intersecting the tube's axis. The detailed results of this study are explained in Section 3.3.4.

3.3.3. Transition characteristics at $Re \approx 1900$

The flow remains steady and laminar for $Re < 1900$. Fig. 7(a) displays the time-series of the fluid temperature at $Re \approx 1900$ and $r/R = 0.70$, along with its phase space and Poincaré section (indicated by the dotted line in the phase space).

Small fluctuations in T_f of frequency slightly less than 1 Hz appear at approximately $Re = 1900$, near the maximum velocity point (that is $r/R \approx 0.7$). These fluctuations are due to the instability of the downward portion of the secondary flow in the lower part of the tube. Fig. 7(b) schematically depicts the instability phenomenon, whose visualization was facilitated by use of incense smoke. The comparatively large fluctuations correspond to right- and left-swaying motion of the downward portion of the secondary flow, indicated by the thick arrow in the figure. The locally spread distribution of trajectory points in the Poincaré section indicates that this unstable flow has a three-dimensional nature. Neither the transition Reynolds number, $Re_{trans} \approx 1900$, nor the transition behavior depends on the fluctuation intensity at the tube inlet, $U_{FI\ in}$.

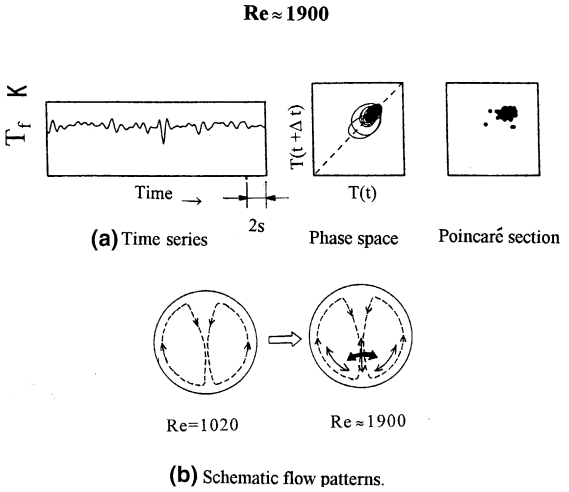

Fig. 7. Time-series of the fluid temperature along with its phase space and Poicaré section at $Re \approx 1900$ and $r/R = 0.70$. (a) Time-series phase space Poincaré section. (b) Schematic flow patterns.

3.3.4. Transition characteristics at $Re = 2230$

In order to understand the mechanisms linked to the occurrence of a particular fluctuation at $Re = 2230$, I attempted to elucidate the transition behavior by analyzing the time-series and profiles. Fig. 8 displays the transitional characteristics at $Re = 2230$.

Fig. 8(a) gives the time dependence of the fluid temperature at various radial locations in the tube, $r/R = -0.86, -0.37, 0.12$ and 0.61. Fig. 8(b) exhibits the instantaneous nondimensional fluid temperature

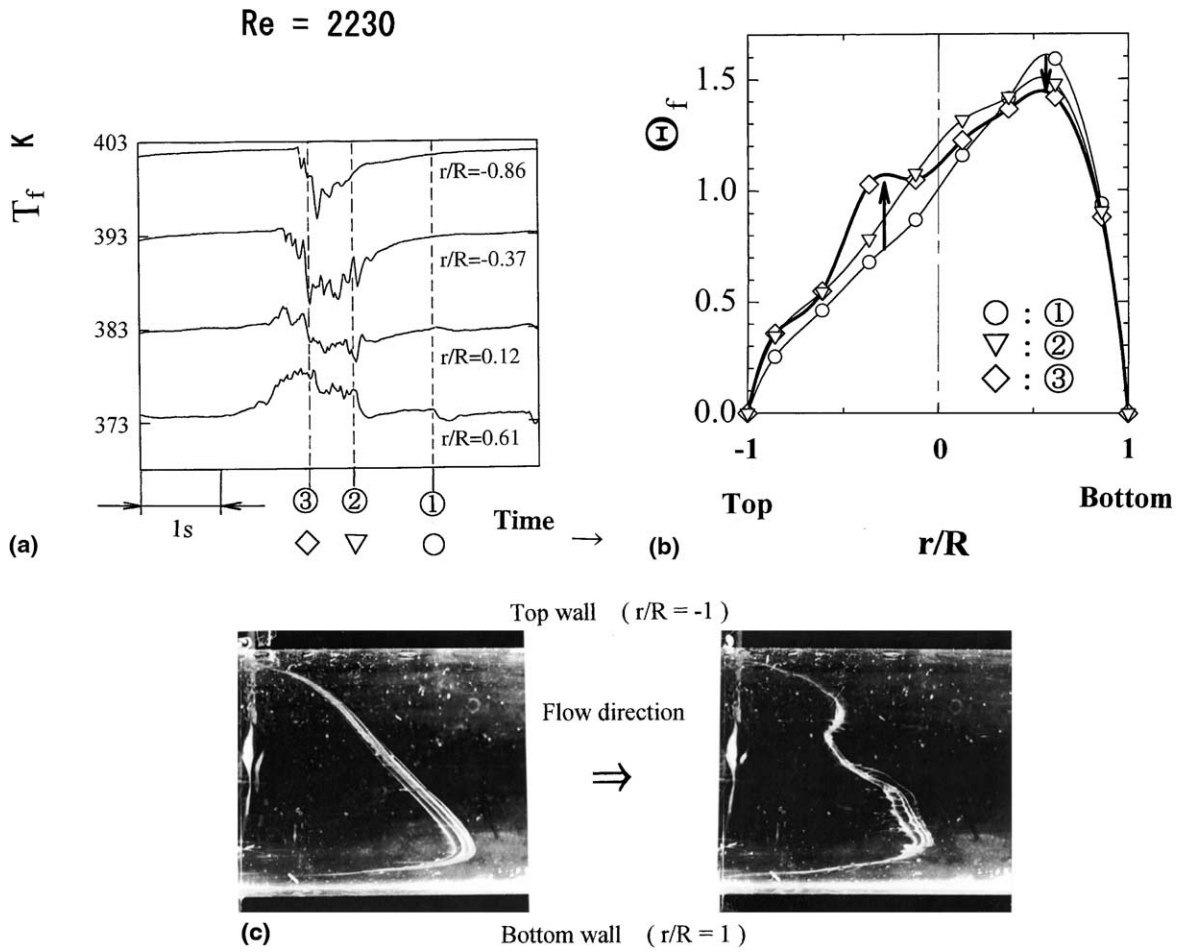

Fig. 8. Transition characteristics at $Re = 2230$. (a) Time-series of the fluid temperature at various radial locations. (b) Instantaneous temperature profiles at different times. (c) Instantaneous flow visualization photos.

profiles Θ_f, determined using the outputs of the eight thermocouples. The times indicated here as ①, ② and ③ correspond to those marked in the same way in Fig. 8(a).

A turbulent lump whose velocity is relatively small and whose fluid temperature T_f is high first appears at $r/R \approx 0.6$ (T_f increases, therefore Θ_f decreases) at a time between ① and ② in Fig. 8(a). This low-velocity lump accelerates the fluid in the upper part (T_f decreases, therefore Θ_f increases) at times ② and ③ around $r/R = -0.4$, and as a result, the downward portion of the secondary flow in the center part of the tube can become destabilized. This causes the appearance of strong temperature fluctuations near $r/R = -0.4$. The instantaneous flow visualization photo displayed in Fig. 8 (c-ii) clearly indicates the acceleration of the fluid near $r/R = -0.4$, while the one displayed in Fig. 8 (c–i) seems to correspond to a laminar Θ_f profile, indicated by the circles in Fig. 8(b).

Fig. 9(a) exhibits time-series of the fluid temperature at various radial locations, and Fig. 9(b) displays a schematic of the corresponding phase space at $Re = 2230$. The trajectory near the maximum velocity point, $r/R = 0.61$, appears as a tangled thread. Contrastingly, the trajectories near the upper part of the tube cross-section, $r/R = -0.86$ to -0.37, exhibit considerably specified linear orbits. Furthermore, the rise and fall of the fluid temperature around $r/R = 0.61$ and -0.37 correspond to the appearance of a low velocity turbulent lump (T_f increases) around $r/R = 0.7$ and the acceleration of the upper part of the fluid (T_f decreases) around $r/R = -0.4$.

3.4. Evidence of chaotic flow

3.4.1. Lyapunov exponents

It is very difficult to judge whether the unstable flow resulting from the instability of the downward portion

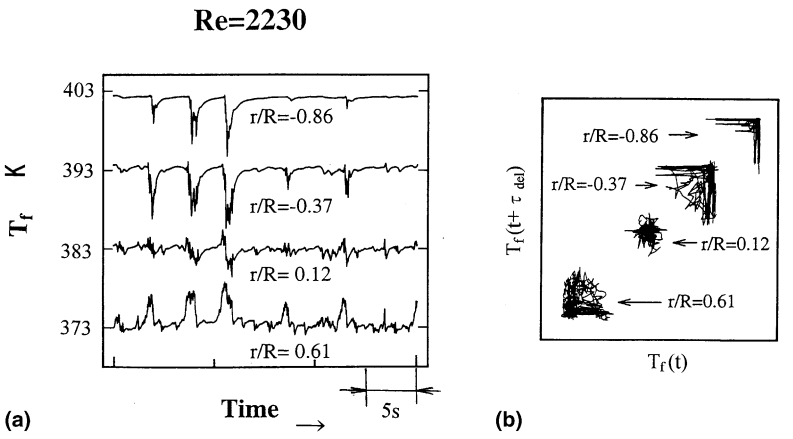

Fig. 9. Time-series of the fluid temperature and its phase space at $Re = 2230$ and various radial locations. (a) Time-series of the fluid temperature at various radial locations. (b) Phase space.

of the secondary flow observed at $Re = 1900$ (shown in Fig. 7) and the small fluctuations that appear near the maximum velocity region at $Re = 2170$ (shown in Fig. 6(b)) is chaotic or not. Because the fluctuation intensity is extremely small ($T_{FI} \leqq 0.4\%$), the level of the signal becomes almost the same as that of the noise.

Fig. 10 displays the time-series (Fig. 10(a)), its power spectra (Fig. 10(b)), and the Lyapunov exponents λ_i for the embedding dimensions $d_m = 6$ and 7 (Fig. 10(c)) at $Re = 2230$. The lower parts of Fig. 10 display the results for the case of the intermittent appearance of turbulent lumps around $r/R = 0.61$, and the upper parts of Fig. 10 display the results for the case of the destabilization of the secondary flow induced by the acceleration of the axial velocity around $r/R = -0.37$. The uncertainties listed for the values of λ_i were determined by several runs, using a variety of τ_{dev} between $3\Delta\tau$ and $6\Delta\tau$ and of N (the number of the phase points within a shell) between 10 and 30.

At $r/R = 0.61$, fluctuation frequencies are below a value of about 10 Hz, and the intensity T_{FI} is about 1.6%. More than three positive Lyapunov exponents appear, and therefore this flow is apparently strongly chaotic. However, the Lyapunov dimension D_L could not be obtained using this algorithm. At $r/R = -0.37$, fluctuation frequencies are below a value of about 10 Hz, and T_{FI} is about 0.8%. Again, more than three positive Lyapunov exponents appear, and the magnitude of the largest positive exponent is about twice that for the unsteady flow at $r/R = 0.61$. This large maximum value of λ_i indicates that the unstable behavior of the trajectory here is stronger for the case of the chaotic flow at $r/R = 0.61$.

3.4.2. Correlation dimension

Fig. 11 shows the relation between the correlation dimension D_c and the embedding dimension d_m for $Re = 2230$ at $r/R = 0.61$ and -0.37. As I see, the value of D_c varies smoothly and converges to a constant value as the embedding dimension is increased. This asymptotic value of D_c, independent of d_m, indicates its own dimension of the attractor. The correlation dimensions of the transitional flow at $r/R = 0.61$, indicated by the triangles, and $r/R = -0.37$, indicated by the solid squares, in the figure are found to be $D_c = 4.0$.

Abid et al. [9,10] reported that when Re goes through Re_{trans}, strong fluctuations appear in the temperature of the tube wall. They found wall temperature behavior that is almost identical to the one found in the present work, as shown in Fig. 9(a). They used Poiseuille flow for the inlet flow by installing an unheated tube length of 1 m (104D), serving as a hydrodynamic approach, at the beginning of the heated section of a horizontal tube with water flow. They also determined the time evolution of the fractal dimension for various Reynolds numbers as a function of the distance along the axial coordinate. In a typical case, they found that the fractal dimension begins with a value greater than 12 near the tube inlet and decreases along the axial coordinate to about 3 in region of the fully developed flow for $Re = 2600$. That is, significantly greater number of degrees of freedom appear at the entrance, and this number decreases as the axial coordinate x increases. They conjectured that this corresponds to the selection and amplification mode by the convection rolls, and that it is as if these temperature fluctuations result from a turbulent instability at the entrance that tends to evolve toward a chaotic state.

In my experiment, I found by direct measurement of the flow field that the transitional time-series, including turbulent lumps, for $Re = 2230$ indicates comparatively low-dimensional chaotic flow with $D_c = 4.0$. It seems that the correlation dimension $D_c = 4.0$ is very

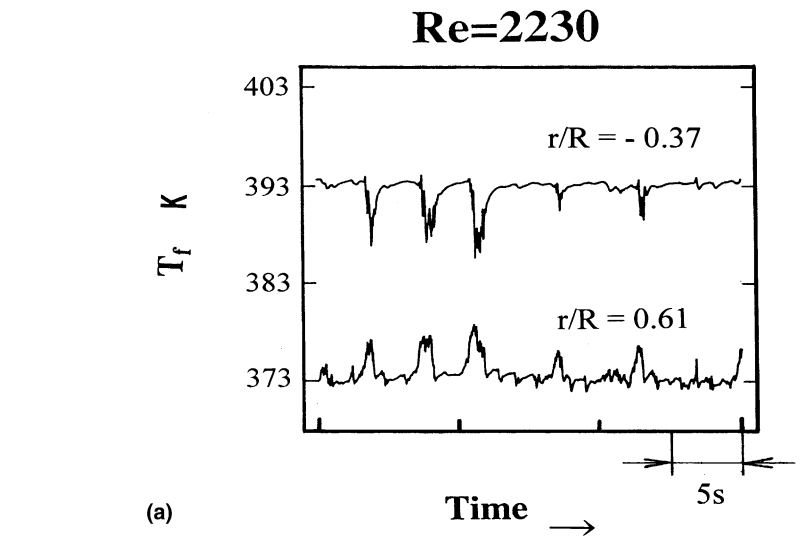

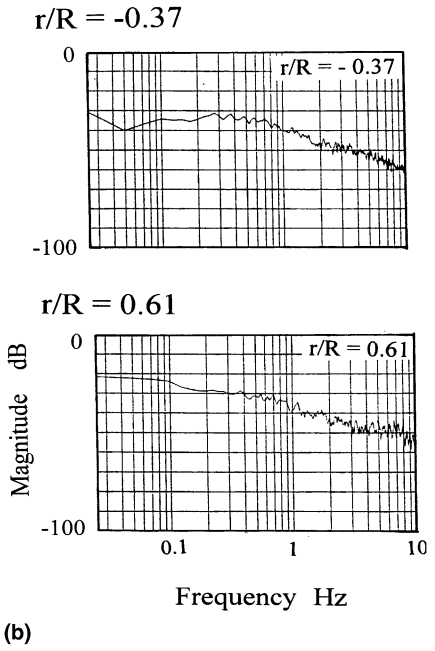

	$d_m = 6$	$d_m = 7$
λ_1	12.2 ± 4	14.8 ± 4
λ_2	5.5 ± 2	8.4 ± 2
λ_3	3.1 ± 1	4.7 ± 2
λ_4	-1.4 ± 1	1.4 ± 1
λ_5	-4.2 ± 3	-1.8 ± 1
λ_6	-11.0 ± 4	-5.3 ± 3
λ_7		-14.0 ± 4

	$d_m = 6$	$d_m = 7$
λ_1	7.7 ± 3	8.7 ± 3
λ_2	7.2 ± 3	8.0 ± 3
λ_3	3.0 ± 2	6.4 ± 3
λ_4	-1.3 ± 1	1.9 ± 1
λ_5	-3.2 ± 2	-1.1 ± 1
λ_6	-9.0 ± 4	-1.8 ± 1
λ_7		-11.4 ± 3

(c)

Fig. 10. Time-series of the fluid temperature, its power spectra, and the Lyapunov exponents. (a) Time-series of the fluid temperature. (b) Power spectra. (c) Lyapunov exponents.

close to an integer but not exactly an integer, because its power spectrum has many peak frequencies which are broadening, and more than three positive Lyapunov exponents appear as shown in Fig. 10. $D_c = 4.0$ is close to Abid's result for $Re = 2600$. In order to determine the transition Reynolds number Re_{trans} and show that the characteristics are almost independent of the velocity fluctuation intensity at the tube inlet. Further investigations from the standpoint of chaos theory that take into consideration the instability due to the heating in the entrance region are certainly needed.

4. Conclusion

I experimentally studied the influence of the buoyancy force and inlet flow conditions on the laminar–

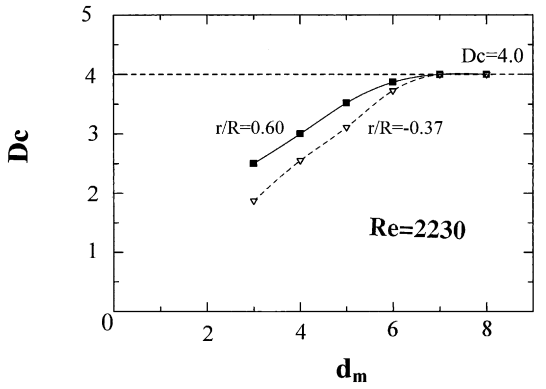

Fig. 11. Correlation dimension.

turbulent transition process of fully developed air flow in a heated horizontal tube with uniform wall heat flux. Experiments were carried out at modified Rayleigh number $Ra_q = 3.1 \times 10^6$, and the conclusions obtained are as follows.

1. For laminar flow, velocity and temperature distributions were obtained, and I found the discrepancies especially in the temperature distributions between these results and those of both the experiment of Mori et al. [14] and the numerical simulation of Ishigaki and Mochizuki [16]. The present results are closer to the latter, which were obtained from simulations using the equations describing only the flow field. However, in order to obtain a more complete understanding of the mixed convection behavior through a numerical study, it is necessary to also include within the model a description of the thermal behavior of the system.
2. Small fluctuations in the temperature below a frequency of about 1 Hz appear near $Re = 1900$, but only near the maximum velocity point, $r/R \approx 0.7$. The appearance of these fluctuations is due to the instability of the downward portion of the secondary flow, and it is independent of the velocity fluctuation intensity at the tube inlet. That is, when Ra_q is large, the secondary flow caused by buoyancy undergoes a transition at Reynolds number Re_{trans}, and the value of Re_{trans} depends little on the fluctuation intensity at the tube inlet.
3. Above $Re = 2230$, turbulent lumps with large fluctuations, whose velocities are relatively small and whose temperatures are high, are first produced at the maximum velocity point $r/R \approx 0.7$. Such a small velocity lump accelerates the fluid in the upper part of the tube around $r/R = -0.4$, and as a result, the downward portion of the secondary flow can become destabilized. Instantaneous flow visualization photos clearly indicate the acceleration of the fluid near the upper part of the tube.
4. The transitional flow at $Re = 2230$ was found to be considerably low-dimensional chaotic nature. This was determined by calculating a set of Lyapunov exponents and the correlation dimension from the time-series of the fluid temperature.

Acknowledgements

The author is grateful to Mr. Kazuto Yamaga, graduate student at the University of Electro-Communications, presently at Fujitsu, for his help with the experiments throughout this work.

References

[1] For example P.R. Fenstermacher, H.L. Swinney, J.P. Gollub, Dynamical instabilities and the transition to chaotic Taylor vortex flow, J. Fluid Mech. 94 (1979) 103–128.
[2] For example J.P. Gollub, S.V. Benson, Many routes to turbulent convection, J. Fluid Mech. 100 (1980) 449–470.
[3] I.J. Wygnanski, F.H. Champagne, On transition in a pipe. Part 1. The origin of puffs and slugs and the flow in a turbulent slug, J. Fluid Mech. 59 (1973) 281–335.
[4] I.J. Wygnanski, M. Sokolov, D. Friedman, On transition in a pipe. Part 2. The equilibrium puff, J. Fluid Mech. 69 (1975) 283–304.
[5] P.R. Bandyopadhyay, Aspects of the equilibrium puff in transitional pipe flow, J. Fluid Mech. 163 (1986) 439–458.
[6] K. Matsuuchi, T. Adachi, Generation of puffs in a pipe, Nagare 12 (1993) 147–156 (in Japanese).
[7] H.R. Nagendra, Interaction of free and forced convection in horizontal tubes in the transition regime, J. Fluid Mech. 57 (1973) 269–288.
[8] M.A. El-Hawary, Effect of combined free and forced convection on the stability of flow in a horizontal tube, J. Heat Transfer 102 (1980) 273–278.
[9] C. Abid, F. Papini, A. Popke, Turbulence et chaos dans un conduit horizontal soumis à un phénomène de convection mixte, Int. J. Heat Mass Transfer 38 (1995) 287–294.
[10] C. Abid, F. Papini, A. Popke, Mixed convection in a horizontal duct; a chaotic system, in: Proceedings of the 10th International Heat Transfer Conference 12-NM-1, 1994, pp. 417–421.
[11] X. Zeng, R. Eykholt, R.A. Pielke, Estimating the Lyapunov-exponent spectrum from short time series of low precision, Phys. Rev. Lett. 66 (1991) 3229–3232.
[12] H. Koizumi, I. Hosokawa, Unsteady behavior and mass transfer performance of the combined convective flow in a horizontal rectangular duct heated from below, Int. J. Heat Mass Transfer 36 (1993) 3937–3947.
[13] P. Grassberger, I. Procaccia, Characterization of strange attractors, Phys. Rev. Lett. 50 (1983) 346–349.
[14] Y. Mori, K. Futagami, S. Tokuda, M. Nakamura, Forced convective heat transfer in uniformly heated

horizontal tubes (1st report experimental study on the effect of buoyancy), Int. J. Heat Mass Transfer 9 (1966) 453–463.
[15] Y. Mori, K. Futagami, Forced convective heat transfer in uniformly heated horizontal tubes (2nd report theoretical study), Int. J. Heat Mass Transfer 10 (1967) 1801–1813.
[16] H. Ishigaki, M. Mochizuki, Fully developed mixed convection in a horizontal pipe, Special Publication of NAL SP14 (1990) 181–185 (in Japanese).